Supplementary Material

Facile Construction of type-I Fe-MOF@g-C_3N_4/BiOI Heterojunction for Boosting Photo-Fenton Catalytic Degradation of Ofloxacin: Performance, DFT Calculations, Pathway, Toxicity assessment and Mechanism

Yunwen Fu[a], Shijie Chen[a,b,*], Ning Liu[a,b], Xiang Li[a,b], Dongxuan Guo[a,b], Xinjia Zhang,[c] Renjiang Lv[a,b], Wencheng Gu[d], Jiaqi Zhang[a]

[a]College of Chemistry and Chemical Engineering, Qiqihar University, Qiqihar 161006, P.R. China

[b]Heilongjiang Provincial Key Laboratory of Catalytic Synthesis for Fine Chemicals, Qiqihar University, Qiqihar 161006, P.R. China

[c]College of Light Industry and Textiles, Qiqihar University, Qiqihar 161006, P.R. China

[d] Network Information Center, Qiqihar University, Qiqihar 161006, P.R. China

Corresponding authors:

*E-mail address: :csj060@163.com; Fax: +86-452-2742575; Tel: +86-452-2742575

Text S1. Characterizations

X-ray diffraction (XRD) (Smart Lab, Rigaku Co., Japan) was used to characterise the crystallographic information of the resulting photocatalysts with a Cu-Kα source (λ= 1.5418 A) at 40 kV and a scan rate of 5° min^{-1}. Fourier transform infrared (FT-IR) spectroscopy (Frontier, PerkinElmer Co., USA) was used to study the functional groups in the photocatalysts. The morphologies of the prepared samples were examined using field emission scanning electron microscopy (SEM) (S-4300, Hitachi Co., Japan) and transmission electron microscopy (TEM) (H-7650, Hitachi Co., Japan) at an accelerating voltage of 200 kV. Using $BaSO_4$ as a standard, the UV-Vis diffuse reflectance spectra (DRS) of the resulting samples were obtained using a UV-Vis spectrophotometer (UV2450, Shimadzu Co., Japan). The samples' room-temperature photoluminescence (PL) spectra were obtained using a photoluminescence detector (F-4500, Hitachi Co., Japan) with an excitation wavelength of 390 nm. The surface elemental composition was measured using X-ray photoelectron spectroscopy (XPS) (ESCALAB 250Xi, Thermo Fisher Co., USA) with monochromatic Al Kα radiation.

Text S2. Testing Methods

The photocatalytic degradation reactor was operated for dark adsorption first, and then the xenon lamp was turned on to allow the photodegradation system to be irradiated under visible light. At regular intervals, 1-2 mL of the degradation solution was withdrawn from the reactor using a syringe. The solution was filtered through a 0.22 μm filter to remove the photocatalyst, and the absorbance of OFX was measured at 292 nm using ultraviolet-visible spectrophotometry. The removal efficiency (R) of OFX was calculated using the following formula:

$$R = \frac{C_0 - C_t}{C_0} \times 100\% \quad (1)$$

where C_0 is the initial concentration of OFX, C_t is the concentration of OFX at time t, and R is the removal efficiency of OFX.

Liquid chromatography-mass spectrometry (LC-MS) (Thermo Scientific Ultimate 3000 UPLC/Q-Exactive Orbitrap MS) the liquid chromatography column employed was a Thermo Scientific Hypersil GOLD C18 Column (50 × 2.1 mm, 1.9 μm). For mass spectrometry analysis, full-scan mode was configured for both positive (ESI^+) and negative (ESI^-) ion detection.

Text S3. Photoelectrochemical Measurements

An electrochemical workstation (CHI 660E, Shanghai, China) was used to evaluate the electrochemical properties of the photocatalysts. A three-electrode system was employed: a saturated calomel electrode (SCE) as the reference electrode, a platinum sheet as the counter electrode, and the photocatalyst deposited on FTO conductive glass as the working electrode. Transient photocurrent response and Mott-Schottky measurements were performed using KCl solution as the electrolyte. Electrochemical impedance spectroscopy (EIS) was tested using $K_3[Fe(CN)_6]$ solution as the electrolyte.

Text S4. DFT calculations

All calculations in this study were performed using the Vienna Ab-initio Simulation Package (VASP) [1]. Spin-polarization effects were incorporated into the periodic density functional theory (DFT) calculations, while the projector-augmented wave (PAW) method was employed to describe the electron-ion interactions, with an energy cutoff of 450.0 eV. The Perdew-Burke-Ernzerhof (PBE) functional, based on the generalized gradient approximation (GGA), was used to account for the exchange-correlation interactions between electrons [2]. Brillouin zone sampling was restricted to the Γ point. To obtain accurate electronic structures, the density of states (DOS) curves were calculated using the HSE06 hybrid functional [3].

Text S5. Equations

The band structures of BiOI and g-C_3N_4 were calculated using the following equations:

$$E(RHE) = E(NHE) + 0.0591pH \quad (2)$$

$$E(NHE) = E(Ag/AgCl) + 0.197 \quad (3)$$

$$E_{VB} = VB - E(RHE) \quad (4)$$

$$E_{CB} = E_{VB} - E_g \quad (5)$$

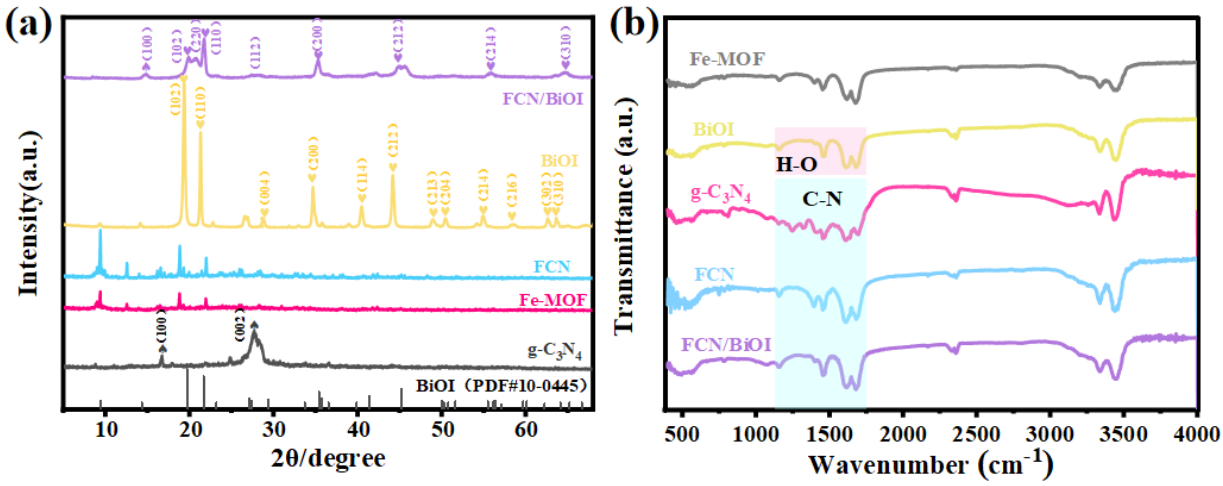

Fig. S1. (a) XRD and (b) FTIR of BiOI、g-C_3N_4、Fe-MOF、FCN and FCN/BiOI

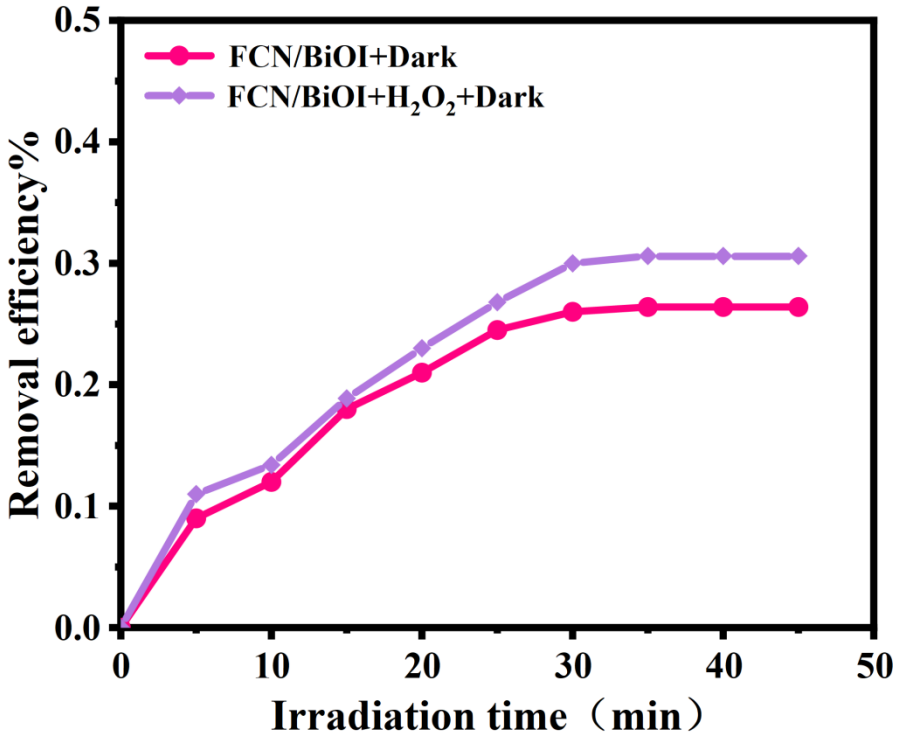

Fig. S2. Performance diagram of OFX removal efficiency by catalyst alone and catalyst-H_2O_2 system under dark conditions.

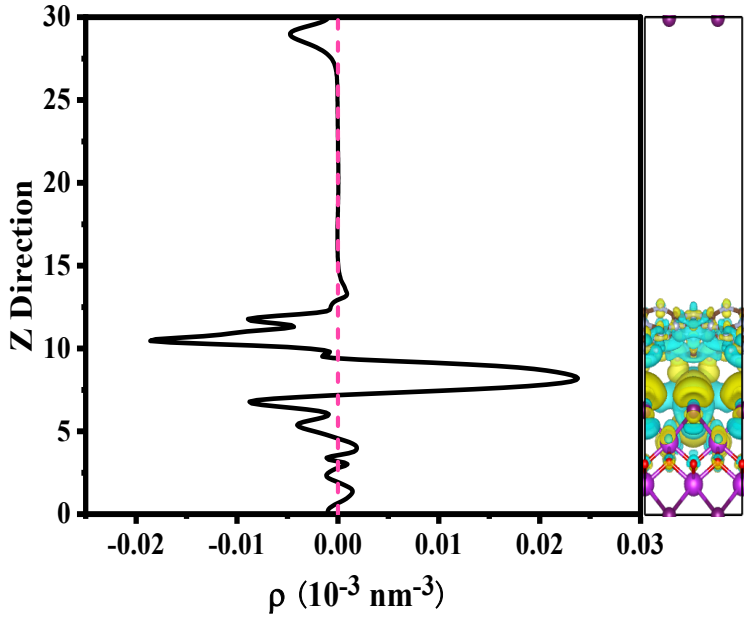

Fig. S3. The planar-averaged charge density difference and 3D charge density difference of BiOI/g-C_3N_4 composites.

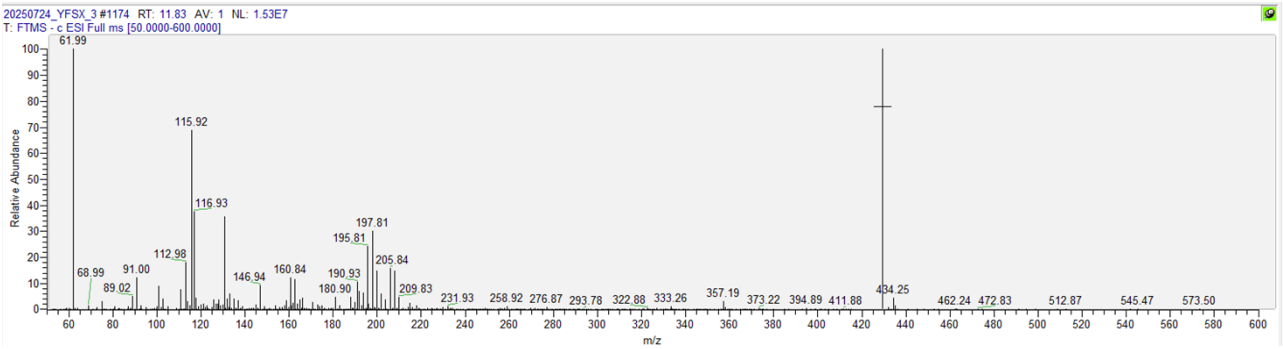

Fig. S4. Mass spectra graphs of OFX degradation.

Table S1. The identified possible intermediate products during OFX degradation from the LC-MS data.

Name	Empirical formula	Exact m/z value (g mol^{-1})	Molecular structure
OFX	$C_{18}H_{20}FN_3O_4$	361	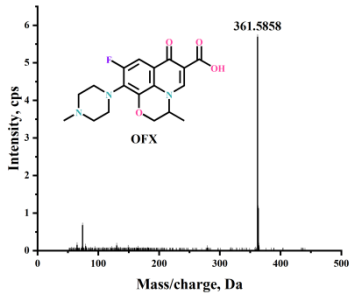
P1	$C_{18}H_{18}FN_3O_6$	391	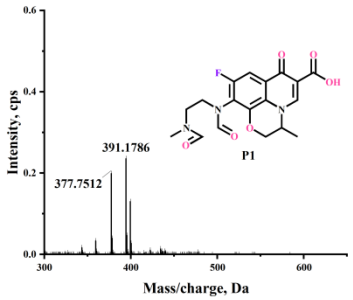
P2	$C_{16}H_{22}FN_3O_4$	339	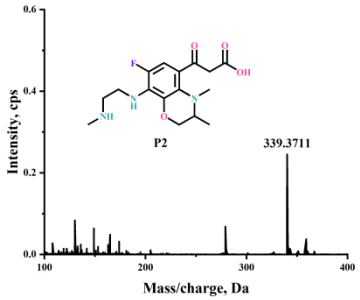
P3	$C_{14}H_{16}FN_3O_2$	277	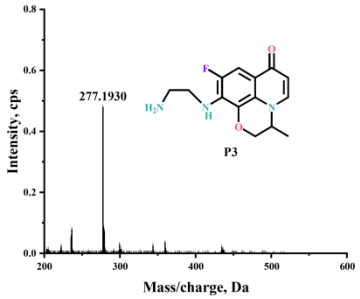

P4	$C_9H_{15}FN_2O_3$	218	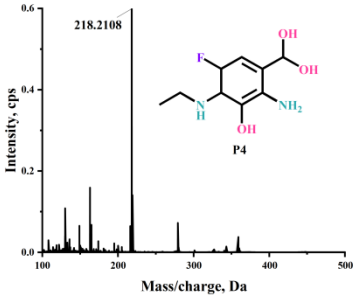
P5	$C_7H_{11}FN_2O_2$	174	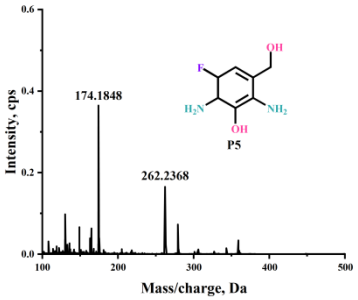
P6	$C_8H_{12}FNO$	158	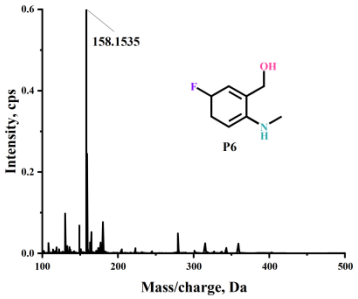
P7	C_7H_9FO	130	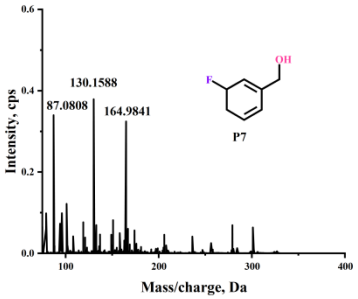

P8	$C_{13}H_{11}FN_2O_4$	278	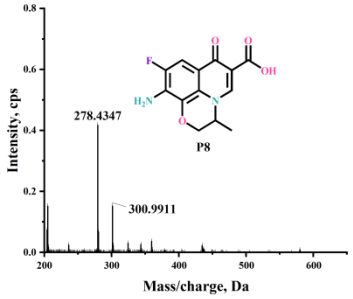
P9	$C_{13}H_{11}FN_2O_3$	262	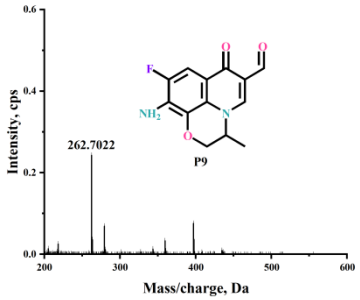
P10	$C_{12}H_{15}FN_2O_3$	255	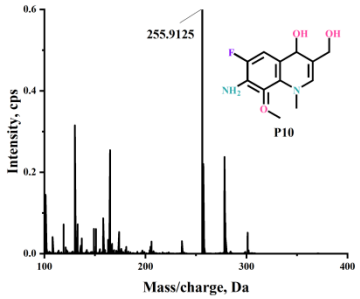
P11	$C_{12}H_{14}FNO_2$	223	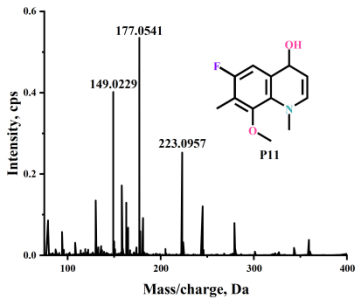

P12	$C_7H_8FNO_3$	174	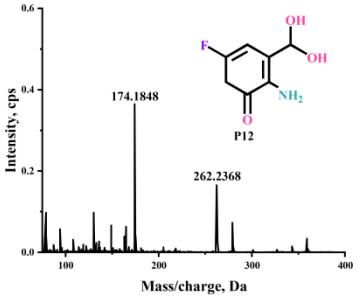
P13	C_6H_8FNO	130	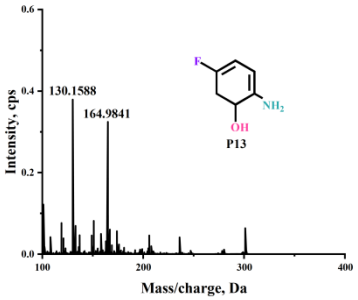

References：

[1] G. Kresse, J. Furthmüller, Comp. Mater.Sci, 1996, 6(1), 15-50.

[2] I. Plowas-Korus, J. Kaczkowski, New J. Chem., 2022, 46(32), 15381-15391.

[3] A.D. Becke, J. Chem. Phys, 2014, 140(18), 18A301.